Chapter 7

H4: Steady Flow through a Channel Network

Contents

7.1 Problem Specification

H4 Steady flow through a simple channel network

Focus network connectivity, steady circulation.

Channel geometry for the Figure 7.1 is listed in Table 7.1. The channel bed-slopes varying from 0 (CF) through 2×10^{-4} in reach AB, 5×10^{-4} in reaches BC, BF and FE, and 10^{-3} in CD. All bed slopes are small and well within the nearly-horizontal flow assumption that is implicit in the conservation Equations 2.4.1 and 2.4.2.

Open boundary conditions are fixed at

$$\eta_A(t) = 0, \quad Q_D(t) = 4,000 \text{ ft}^3/\text{s}, \quad Q_E(t) = 2,000 \text{ ft}^3/\text{s} \qquad \text{for all } t > 0 \tag{7.1.1}$$

Use a fixed computational space step $\Delta x = 500$ ft and a fixed computational time step $\Delta t = 30$ s.

Compute and write to file in the STANDARD FORMAT the initial conditions at $t = 0$ and the model predictions for EVERY[1] time step to STEADY STATE.

[1]For most choices of initial conditions, the time to steady state is about ten hours. The data files are very large

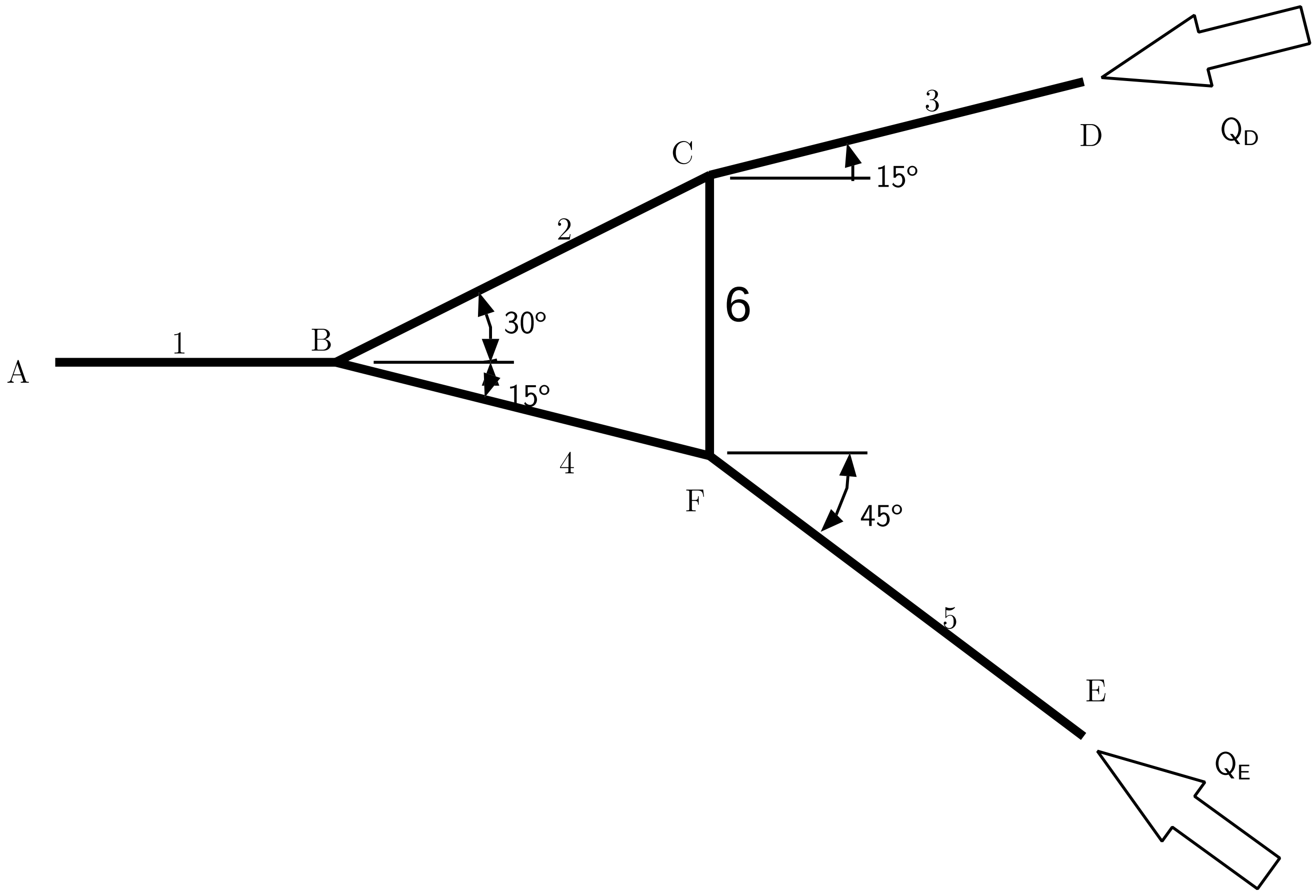

Figure 7.1: Schematic Network.

Reach	#1/AB	#2/BC	#3/CD	#4/BF	#5/FE	#6/CF
B ft	400	300	300	200	200	100
L ft	25,000	10,000	10,000	10,000	10,000	10,000
f	0.02	0.025	0.025	0.03	0.03	0.04
n	0.016	0.018	0.018	0.02	0.02	0.03
Node	A	B	C	D	E	F
Z ft	-20	-15	-10	+0	-5	-10

L is reach length.

Table 7.1: **Channel geometry for Schematic Network**

and surface plots are very dense. For the following presentations, data file entries every 300 s to 30,000 s have been plotted.

7.2 Background

Networks of tidal channels become parallel computations in the separate reaches. But these parallel computations are coupled for all times by *compatibility conditions* at each of the network nodes.

For the network in Figure 7.1, boundary conditions must be specified at each end of each reach. Specifically,

- open boundary conditions at A, D and E. These are the η and Q conditions in Equations 7.1.1.
- internal (but still "open") boundary conditions at B, C and F. These are the compatibility conditions.

The specific compatibility conditions at channel junctions would normally be

1. water surface elevation is the same for all channels at each junction for all time
2. vector sum of flow into each junction is zero for all time

The water surface compatibility conditions become

$$\begin{aligned} \eta_{AB}(x_B,t) &= \eta_{BC}(x_B,t) = \eta_{BF}(x_B,t) \\ \eta_{BC}(x_C,t) &= \eta_{CD}(x_C,t) = \eta_{CF}(x_C,t) \\ \eta_{BF}(x_F,t) &= \eta_{FE}(x_F,t) = \eta_{CF}(x_F,t) \end{aligned} \tag{7.2.1}$$

The flow compatibility conditions become

$$\begin{aligned} Q_{AB}(x_B,t) - Q_{BC}(x_B,t) - Q_{BF}(x_B,t) &= 0 \\ Q_{BC}(x_C,t) - Q_{CD}(x_C,t) - Q_{CF}(x_C,t) &= 0 \\ Q_{BF}(x_F,t) - Q_{FE}(x_F,t) + Q_{CF}(x_F,t) &= 0 \end{aligned} \tag{7.2.2}$$

To be strictly consistent with the hydrodynamic Equations 2.4.1 and 2.4.2, each junction would be a finite storage volume and the compatibility conditions should be mass and vector momentum conservation. Equations 7.2.1 and 7.2.2 specifically assume zero storage volume and gradually-varied flow at the junction. The present test investigates the impact of these internal compatibility conditions on the evolution to a steady network flow.

7.3 Contra Costa Water District

CCW changed the coordinate system and the reach numbering from Figure 7.1 and Table 7.1. Table 7.2 provides the mapping that was apparently adopted by CCW and its relationship to the Table 7.1 network layout. Reference to Tables 7.1 and 7.2 will assist in comparative interpretation

Reach	1	2	3	4	5	6
Standard	AB	BC	CD	BF	FE	CF
CCW	AB	BC	BF	FC	CD	FE

Order of nodes identifies positive flow direction

Table 7.2: Translation of CCW Network Layout

of the CCW predictions.

Figures 7.2 and 7.3 shows the CCW-predicted η and Q evolution toward the steady state. The response patterns show the expected transient evolution through t_L = 30,000 s. The immediately noticeable feature of these response patterns is initial transient oscillations. These are generated by the rapid transition from assumed initial conditions to the Equation 7.1.1 boundary conditions. As expected, they decay slowly due to friction. By 30,000 s, steady state is approached, but not completely reached. The CCW data file has predictions through 90,000 s, but these are still not at steady state. There is a hint of a problem here.

On closer perusal however, there is unmistakable evidence of a serious problem. For Reach 3 at steady state, the flow should be constant throughout the reach. The CCW-predicted flow increases from -4000 ft^3/s at D to about -4600 ft^3/s at C. This is not a steady flow, and is should force a very significant response in the coupled water surface evolution. But there is no response in the η predictions (Reach 3 in Figure 7.2).

In addition, mass is not conserved for the entire system. Internal storage at t_L seems to be zero from Figure 7.2, so that inflows to the system and outflows from the system must balance at t_L. They do not; inflows are 4,000 ft^3/s at D (Reach 3 at x = 10,000 ft) and 2,000 ft^3/s at E (Reach 5 at x = 10,000 ft), but the outflow appears to be 6,500 ft^3/s at A (Reach 1 at $x = 0$).

The gradually-varied water surface profile at t_L is shown in Figure 7.4, Visually, this seems to be the expected response. There is a gradually-varied M_2-type backwater curve extending upstream from A. As expected, the steepest profile, in reach CD, corresponds to the steepest bed slope. Visually also the vector flow field at t_L, in Figure 7.5, seems to be the expected response. The mass balance problems identified with Figure 7.3 are masked by the scale of the plot.

Figure 7.6 shows the instantaneous flow or mass balances at junctions B, C and F. This is the expected response, and mass is conserved at the junctions throughout.

Figure 7.7 shows the associated water surface elevations at junctions B, C and F. For each junction, the water surface elevations vary with time but remain consistent. This also is the expected response.

Collectively, Figures 7.6 and 7.7 confirm the network coding, and suggest that the source of the spatially-varied flow in Reach 3 at "steady state" must lie elsewhere.

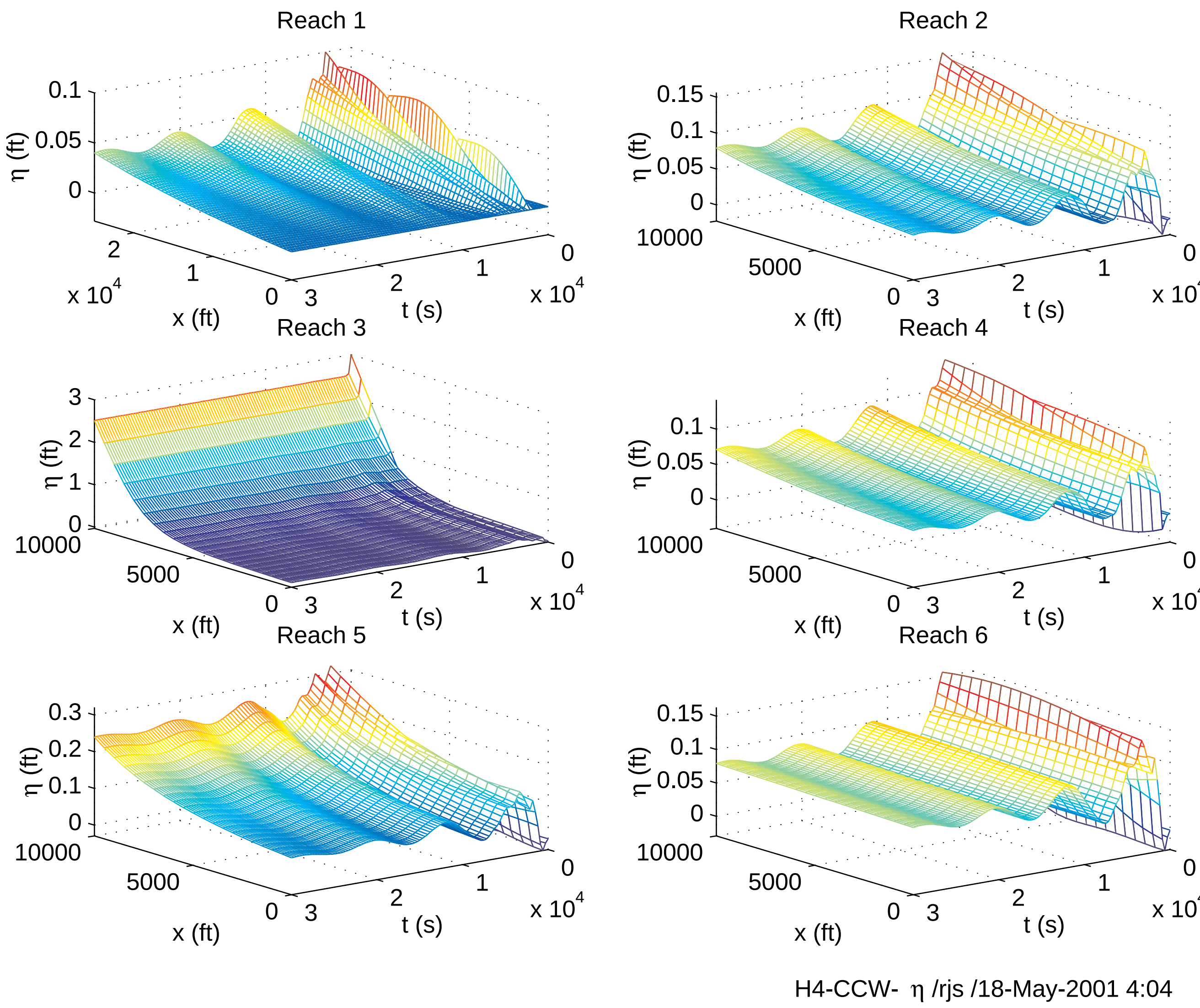

Figure 7.2: H4 CCW-predicted η solution field evolution.

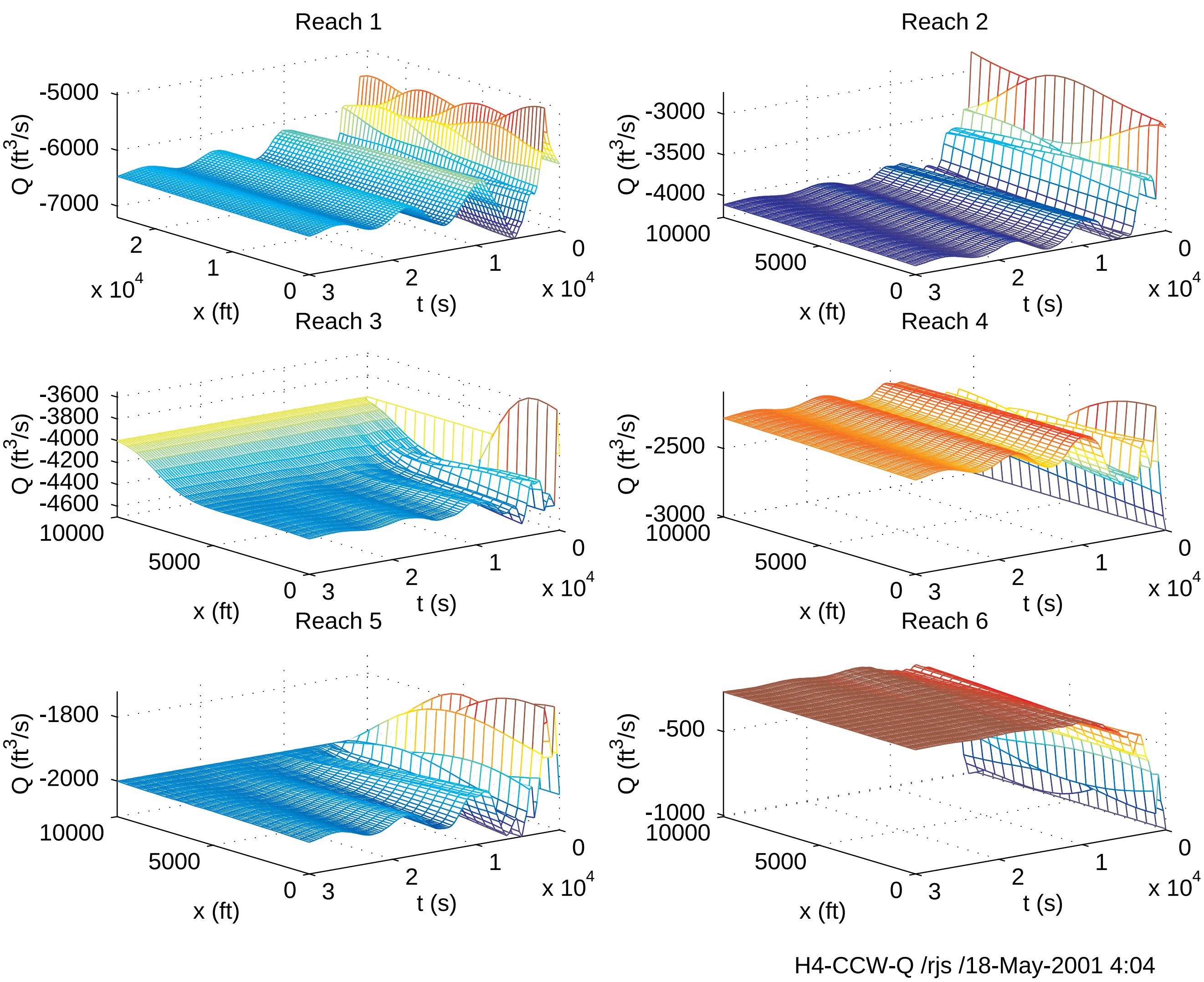

Figure 7.3: H4 CCW-predicted Q solution field evolution.

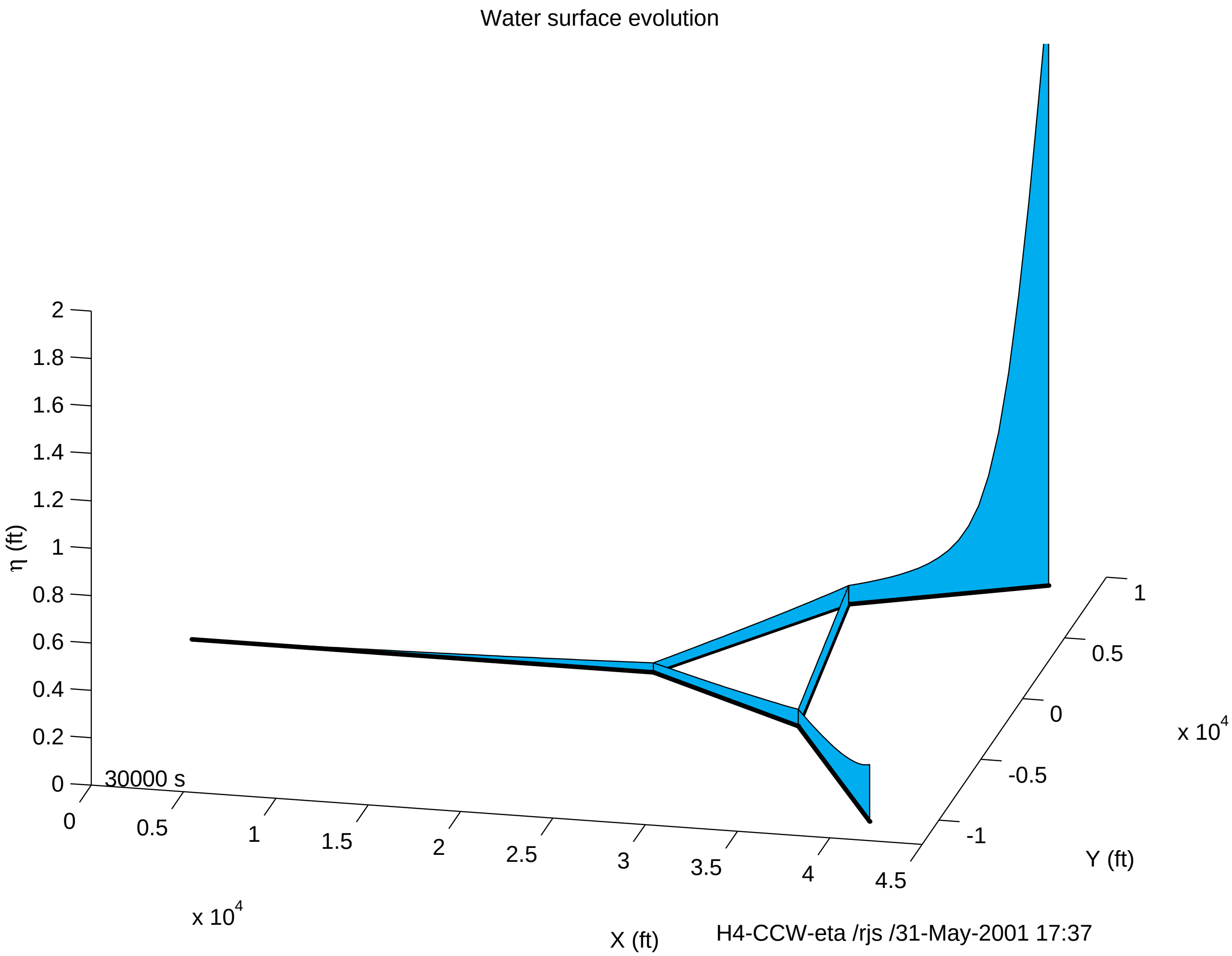

Figure 7.4: H4 CCW-predicted $\eta(x, t_L)$ solution field at $t_L = 30{,}000$ s.

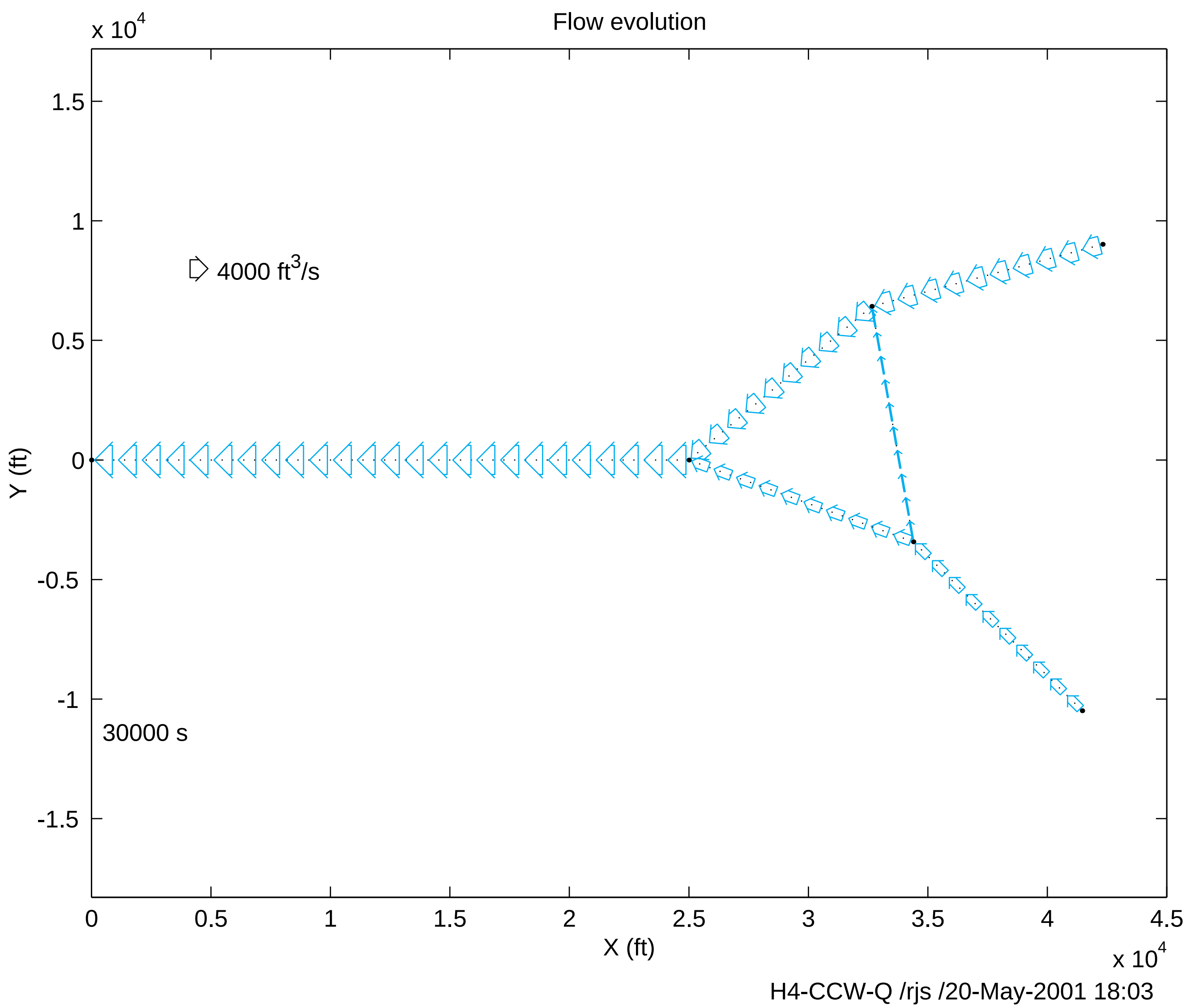

Figure 7.5: H4 CCW-predicted $Q(x, t_L)$ solution vector field at $t_L = 30{,}000$ s.

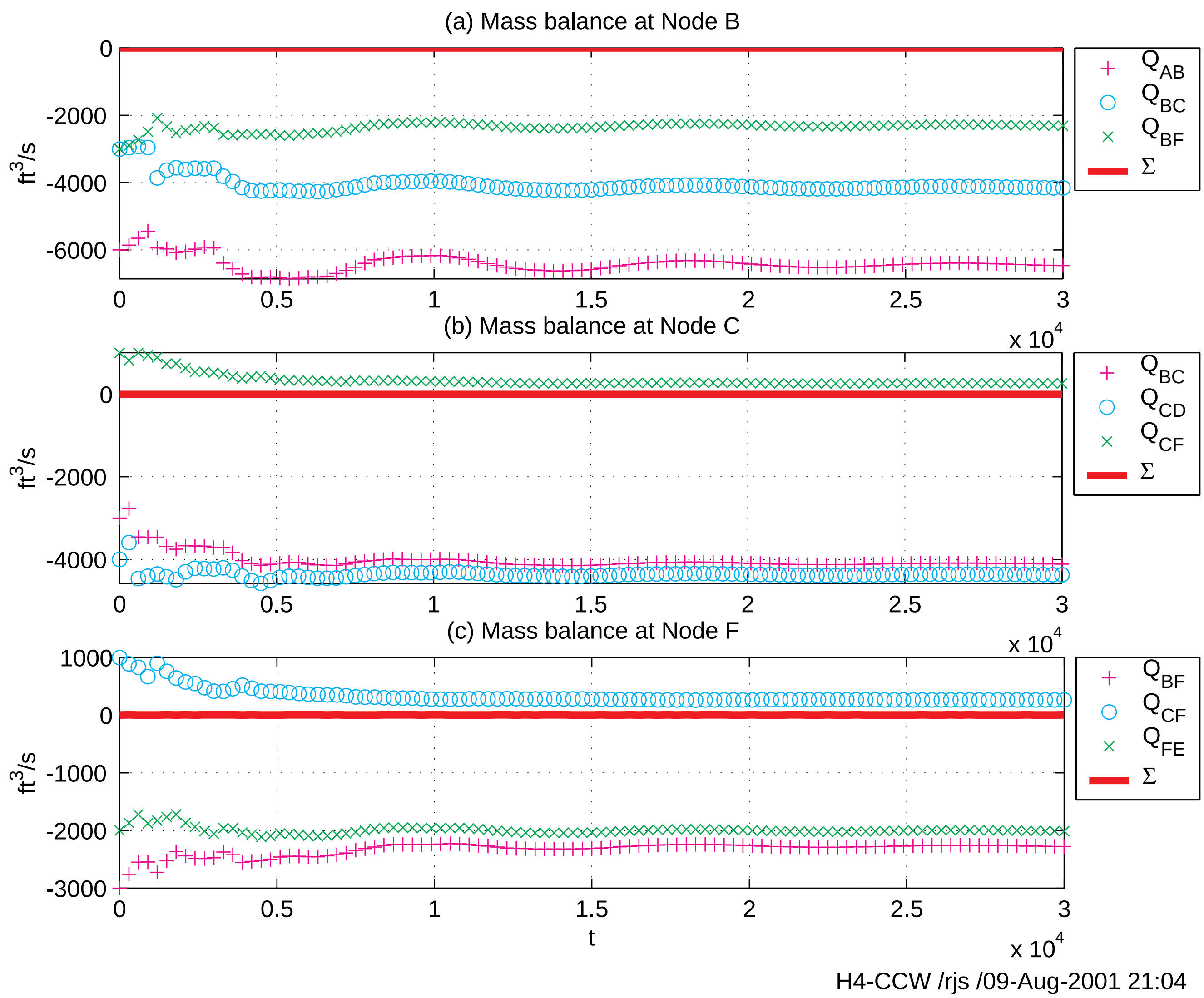

Figure 7.6: H4 CCW-predicted mass balances at network nodes.

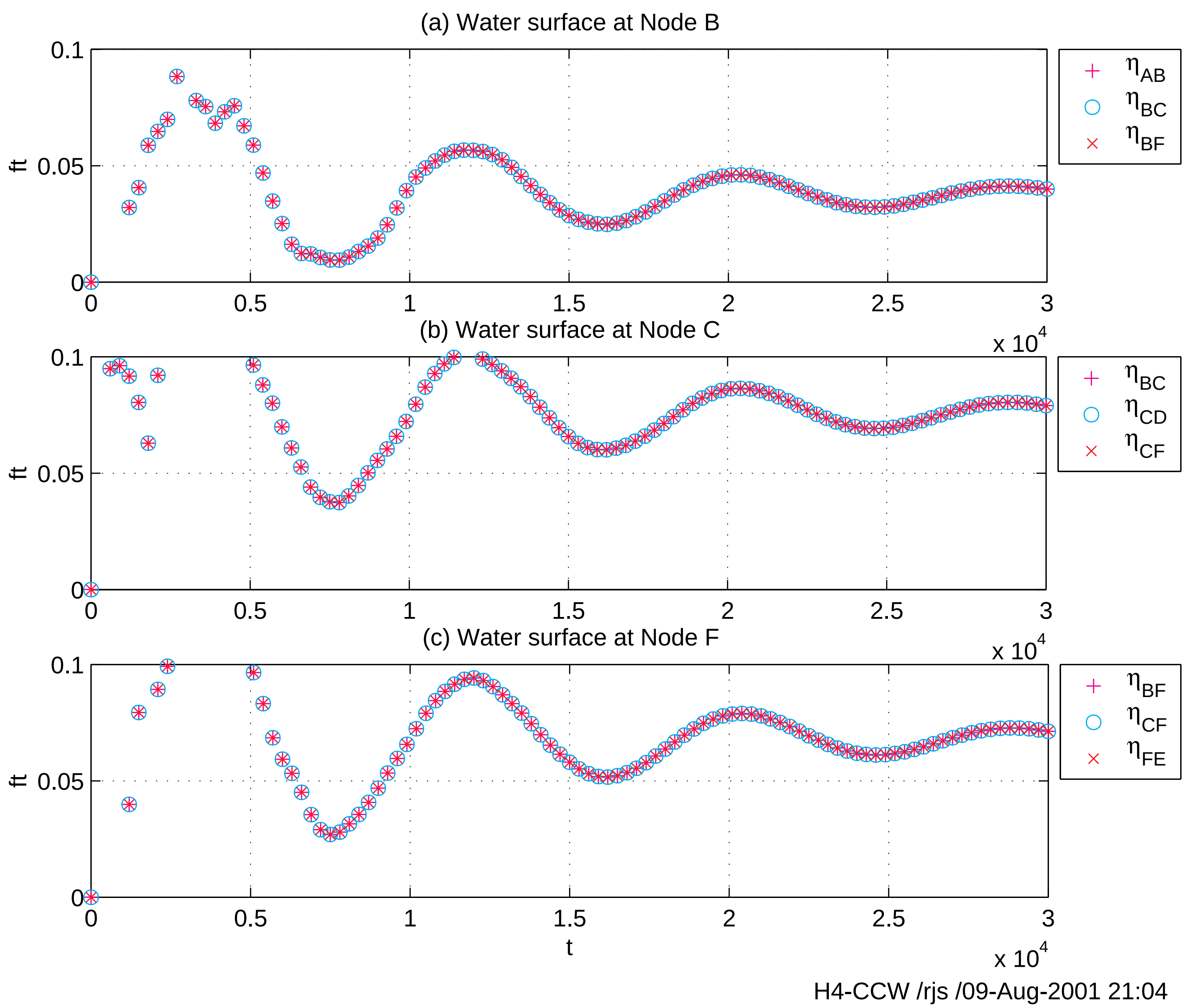

Figure 7.7: H4 CCW-predicted water surface elevation at network nodes.

CCW[2] attribute this error to a "leakage (difference between flow into and out of the channel)" which is "likely due to the large truncation error in the first-order (in space) numerical scheme when the longitudinal gradient in water depth is large."

But all bed slopes are small, in particular 5×10^{-4} in reaches BC, BF and FE, and 10^{-3} in CD. And water surface slopes are also small; CCW cite 4.7×10^{-4} in reach CD. These are well within the nearly-horizontal flow assumption that is implicit in the conservation Equations 2.4.1 and 2.4.2. If truncation error is the cause, then the CCW model has exceeded the limits of its applicability. While bed and water surface gradients in typical Delta flows may be much milder, scenarios that would involve less tranquil flows, embankment failures for example, will need to be carefully reviewed.

[2]The following commentary was provided by CCW (Shum, 27 April 2001): "The leakage is most likely due to the large truncation error in the first-order (in space) numerical scheme when the longitudinal gradient in water depth is large. At the end of the 25-hour simulation, the surface elevation along channel CD decreases from 2.5' at the upstream end to 0.1' at the downstream end. With a channel slope of 0.001, the water depth actually increases from 2.5 to 10.1 . The longitudinal gradient of the water depth (or surface slope in a reference frame with the vertical axis normal to channel bottom) is most pronounced in the upstream half, where it averages 0.00047 (compared with a bottom slope of 0.001) over the distance of 5,000'. The leakage over this 5000' is 365 cfs, accounting for over 99% of the error in mass balance (leakage) in the 10,000' channel.

A separate simulation using the Fischer Delta Model with bottom slope set to zero (all channel bottoms at -20' relative to datum), and hence the longitudinal gradient in water depth is much smaller in channel CD, showed no leakage. That is, flows at the two ends of channel CD were both at 4,000 cfs. Leakage (difference between flow into and out of the channel) in all other channels are also zero.

The following table shows the results of additional simulations. The leakage decreases monotonously (approximately linearly) as the grid size decreases (the time step in each simulation is decreased accordingly to keep the Courant number unchanged). This affirms that the problem is truncation error.

Percentage Error in Flow			
	Channel		
Grid Size	AB	CD	FE
500'	7.9%	9.2%	0.3%
250'	3.9%	4.5%	0.2%
125'	1.9%	2.2%	0.1%

Percentage Error in Flow is the difference between outflow and inflow as a percentage of inflow (outflow) for a channel with inflow (outflow) imposed as boundary condition or as a requisite for global mass balance."

7.4 Department of Water Resources

DWR changed[3] the coordinate system and the reach numbering from Figure 7.1 and Table 7.1. Table 7.3 provides the mapping that was apparently adopted by DWR and its relationship to the Table 7.1 network layout. Reference to Tables 7.1 and 7.3 will assist in comparative interpretation

Reach	1	2	3	4	5	6
Standard	AB	BC	CD	BF	FE	CF
DWR	EF	FB	FC	DC	CB	BA

Order of nodes identifies positive flow direction

Table 7.3: Translation of DWR Network Layout

of the DWR predictions.

Figures 7.8 and 7.9 shows the DWR-predicted η and Q evolution toward the steady state. The response patterns show the now expected transient evolution through $t_L = 30{,}000$ s. The transient oscillations are initially strong and decay with time. By 30,000 s, steady state is approached, but not completely reached. The DWR data file has predictions through 129,600 s. At this time, the network flow is clearly at steady state.

The gradually-varied water surface profile at t_L is shown in Figure 7.10, and the vector flow field also at t_L in Figure 7.11. These are the expected response patterns.

Figure 7.12 shows the instantaneous flow or mass balances at junctions B, C and F. This is the expected response, and mass is conserved at the junctions throughout.

[3] In addition, the time step Δt is reported in the DWR data files as 1 s; it was apparently not the specified 30 s, but 60 s. The time step has been changed to 60 s for the following analyses.

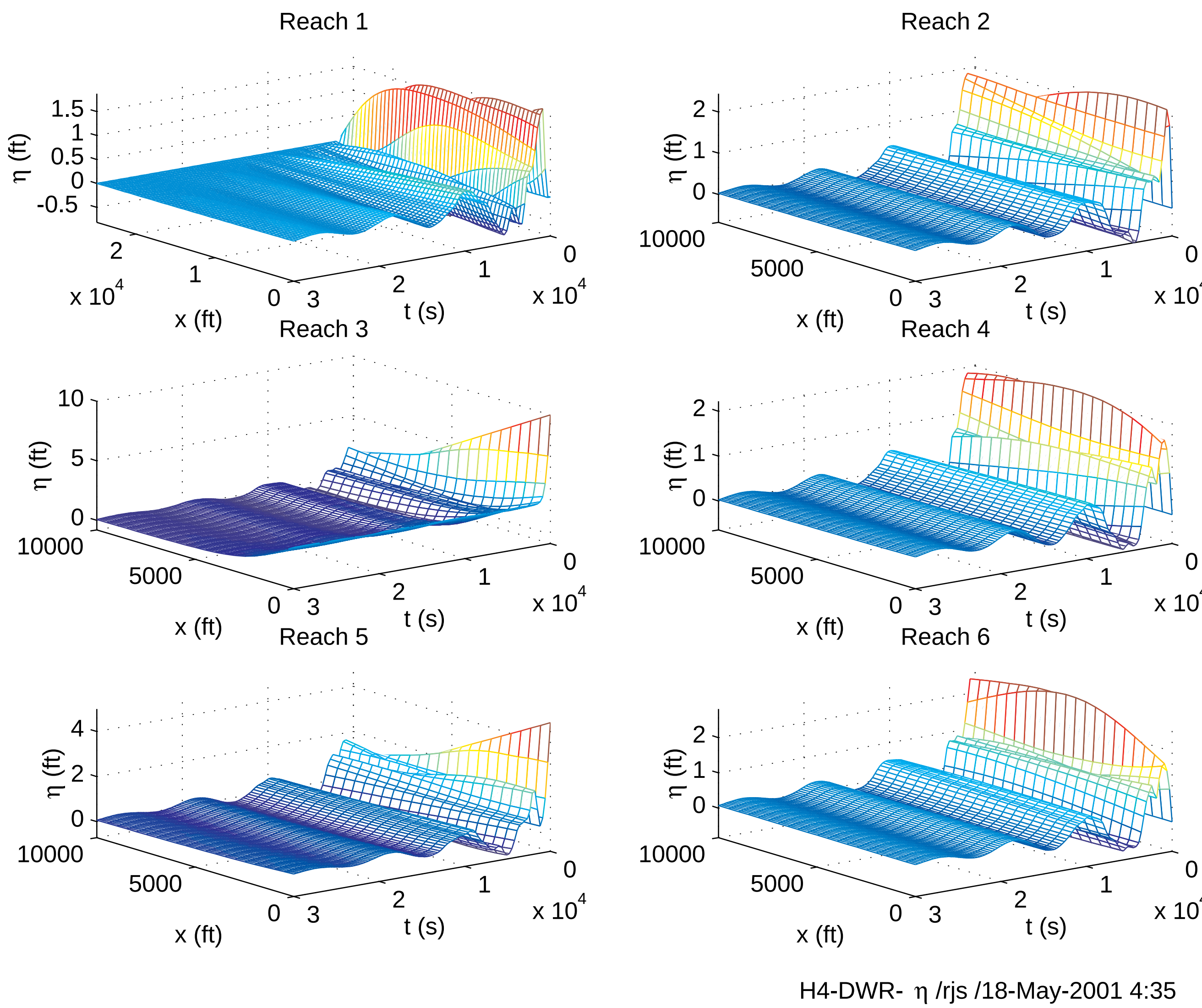

Figure 7.8: H4 DWR-predicted η solution field evolution.

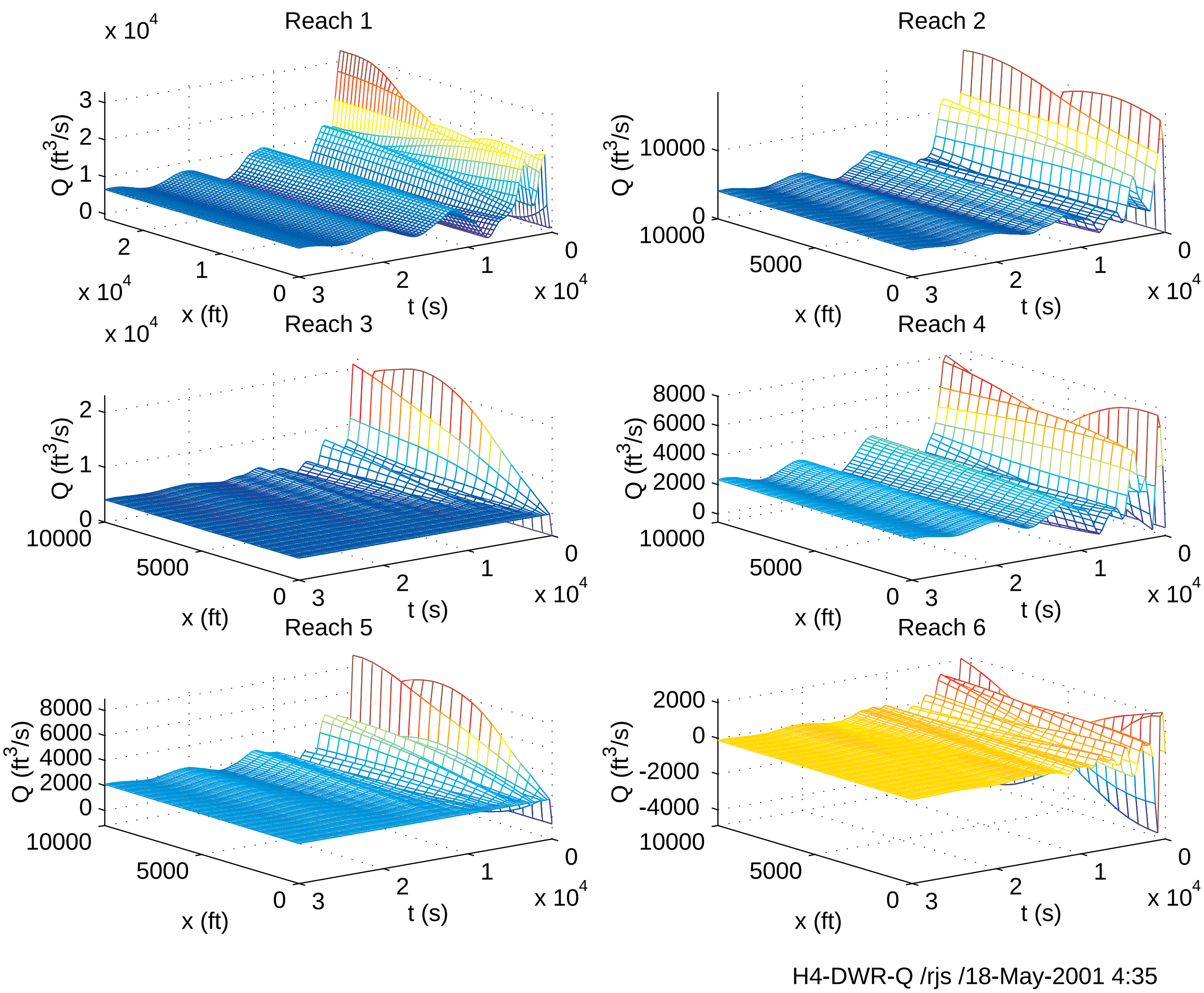

Figure 7.9: H4 DWR-predicted Q solution field evolution.

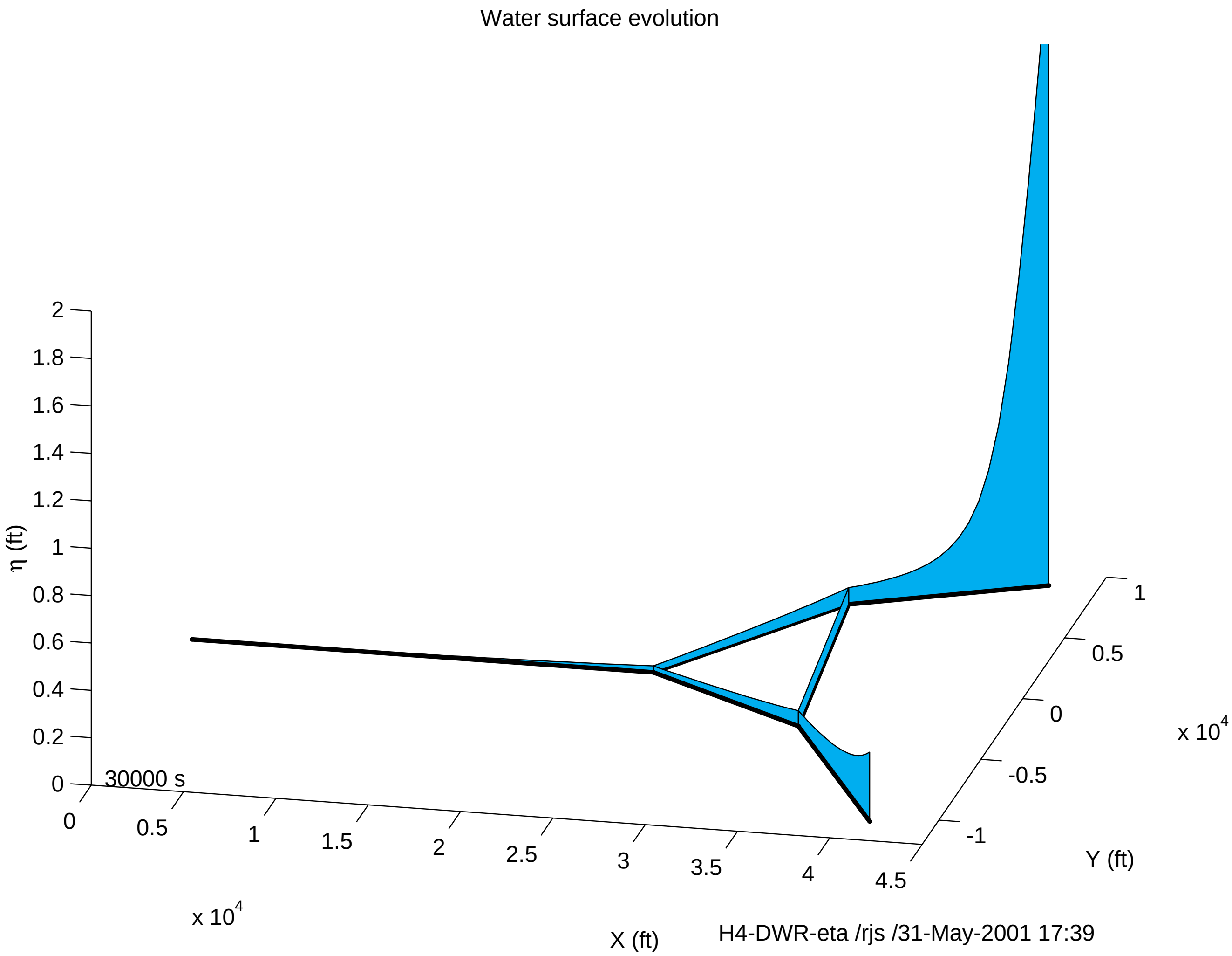

Figure 7.10: H4 DWR-predicted $\eta(x, t_L)$ solution field at $t_L = 30{,}000$ s.

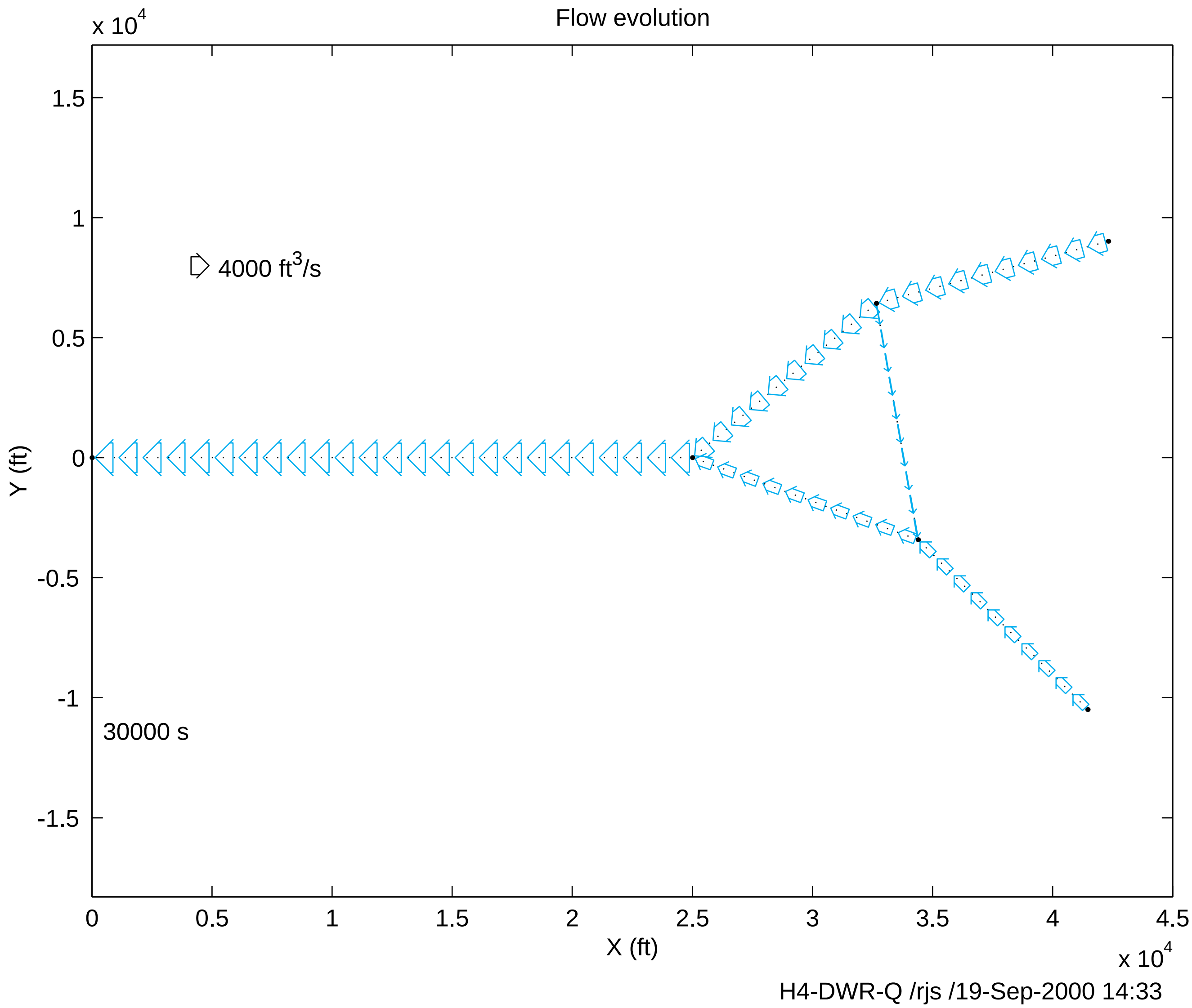

Figure 7.11: H4 DWR-predicted $Q(x, t_L)$ solution vector field at $t_L = 30{,}000$ s.

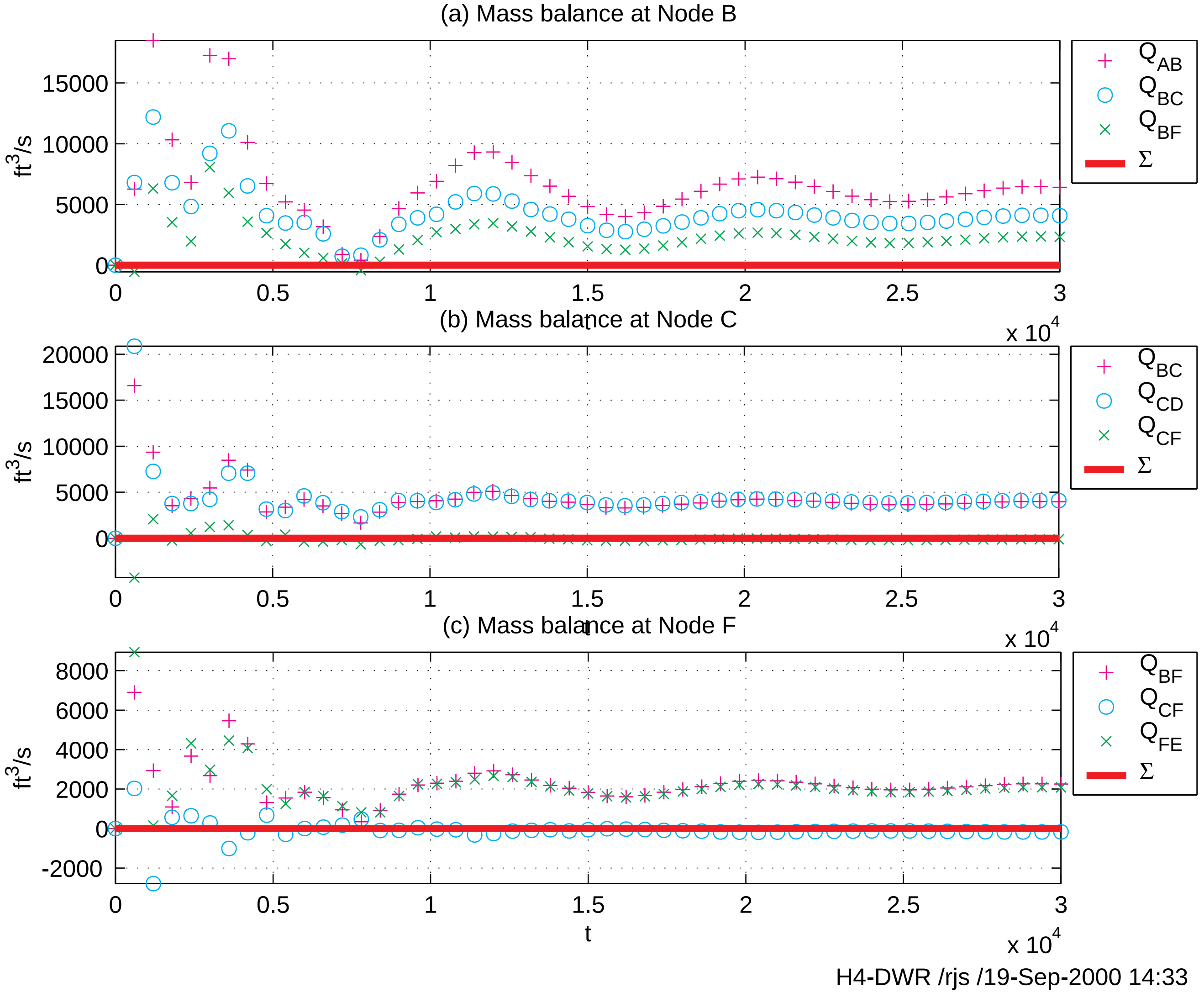

Figure 7.12: H4 DWR-predicted mass balances at network nodes.

7.5 Resource Management Associates

Figures 7.13 and 7.14 shows the RMA-predicted η and Q evolution toward the steady state. The response patterns show the expected transient evolution through $t_L = 30{,}000$ s. The transient oscillations are initially strong and decay with time. By 30,000 s, steady state is approached, but not completely reached.

The RMA data file has predictions through 89,996 s. At this time, the network flows are steady to only two significant figures. Residual oscillations in the third significant figure persist in a manner suggestive of grid-scale oscillations. Such oscillations are often indicative of a less-than-satisfactory numerical algorithm. Previous observations of this response pattern have perhaps been observed in Figures 5.10b, 6.8d, 6.9c and d.

The gradually-varied water surface profile at t_L is shown in Figure 7.15, and the vector flow field also at t_L in Figure 7.16. Visually, these are at steady state.

Figure 7.17 shows the instantaneous flow or mass balances at junctions B, C and F. This is the expected response, mass being conserved at all three junctions.

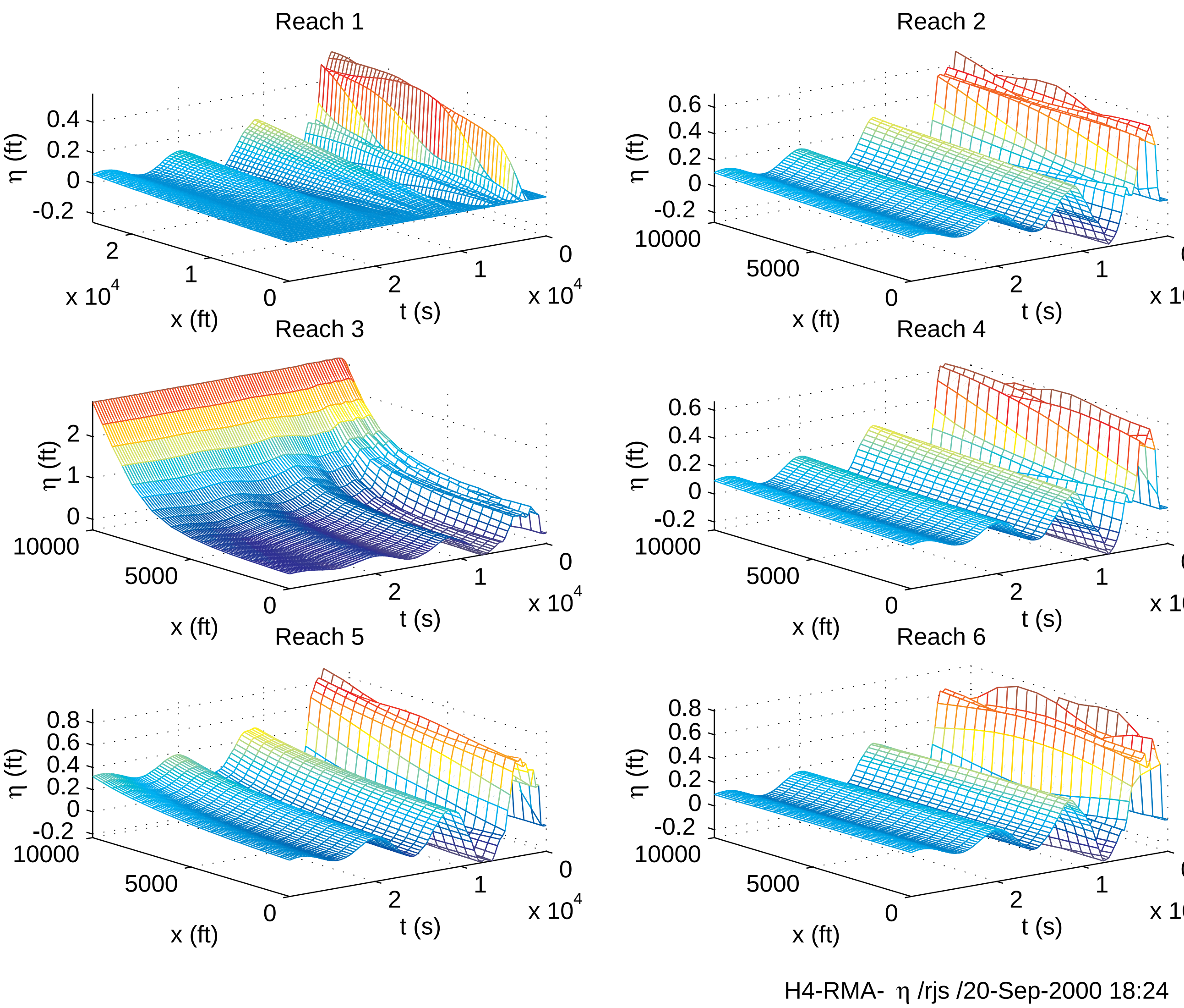

Figure 7.13: H4 RMA-predicted η solution field evolution.

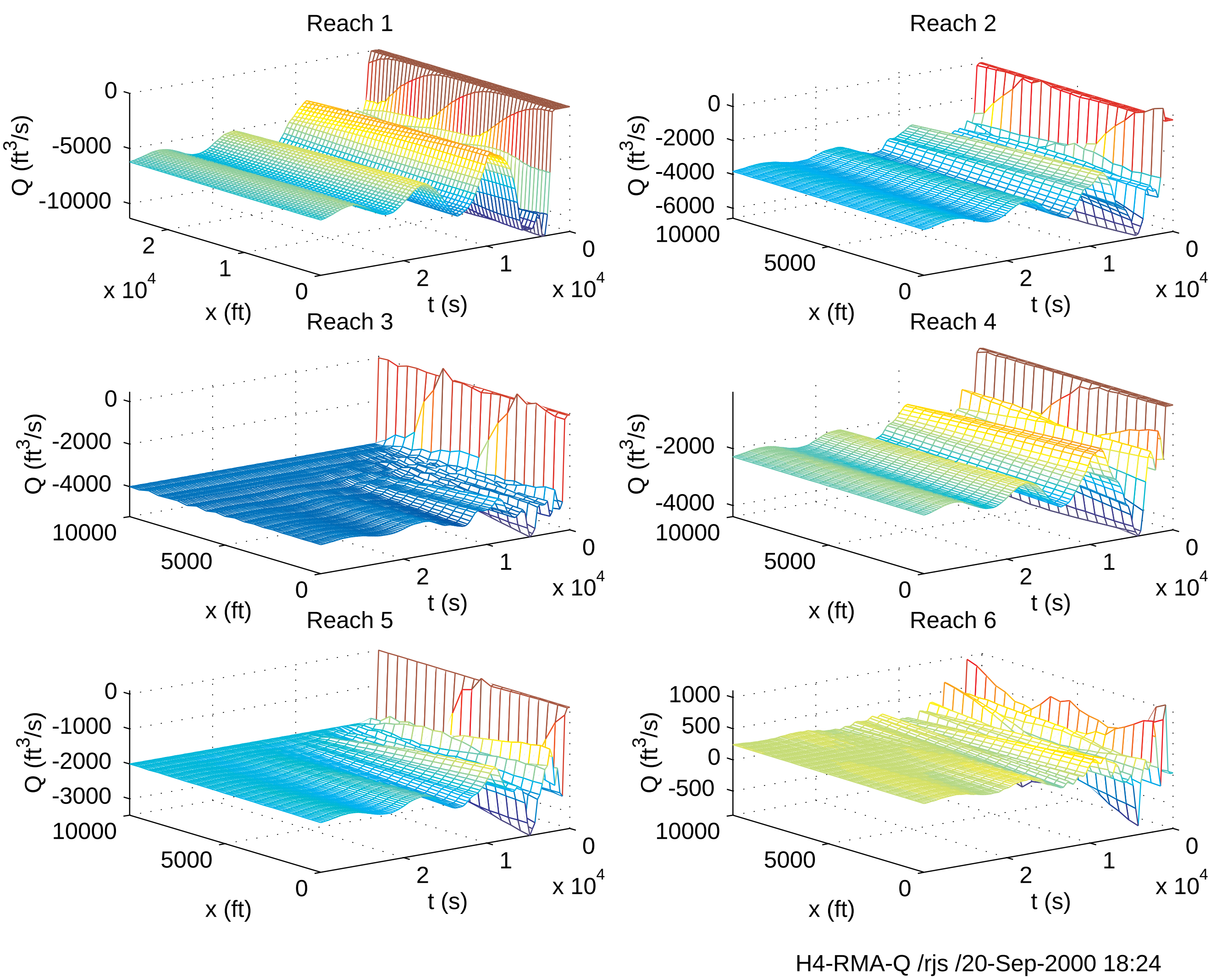

Figure 7.14: H4 RMA-predicted Q solution field evolution.

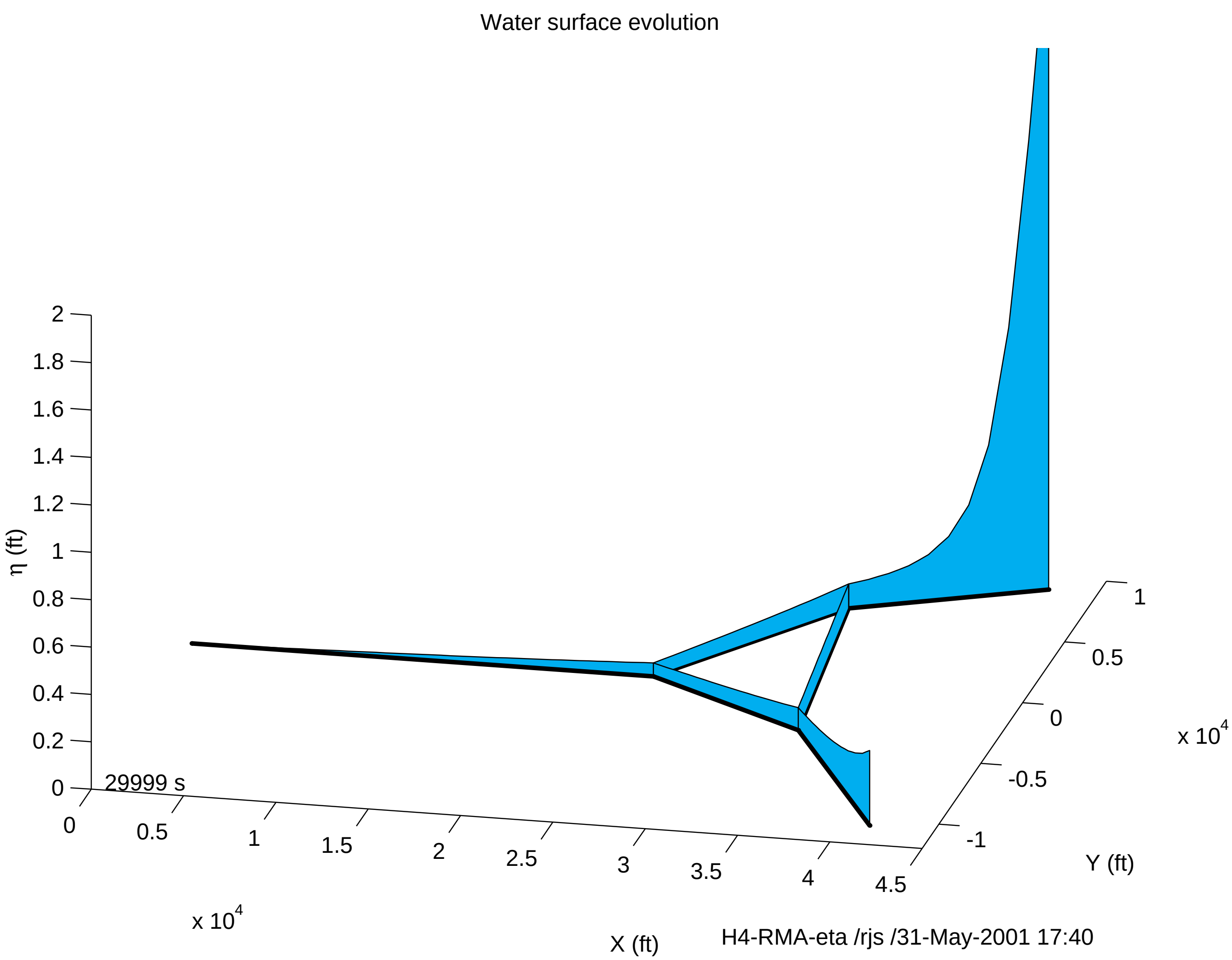

Figure 7.15: H4 RMA-predicted $\eta(x, t_L)$ solution field at $t_L = 30{,}000$ s.

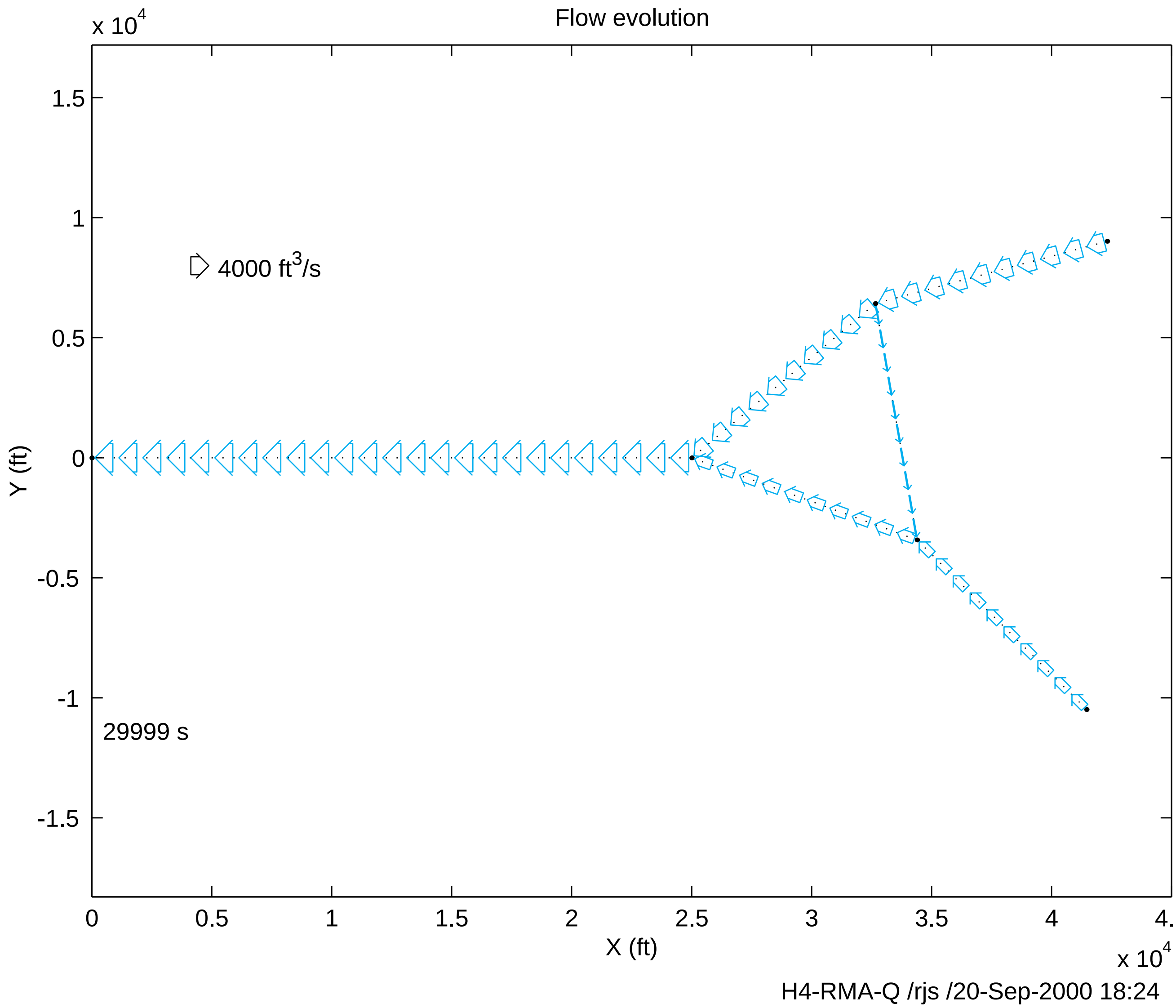

Figure 7.16: H4 RMA-predicted $Q(x, t_L)$ solution vector field at $t_L = 30{,}000$ s.

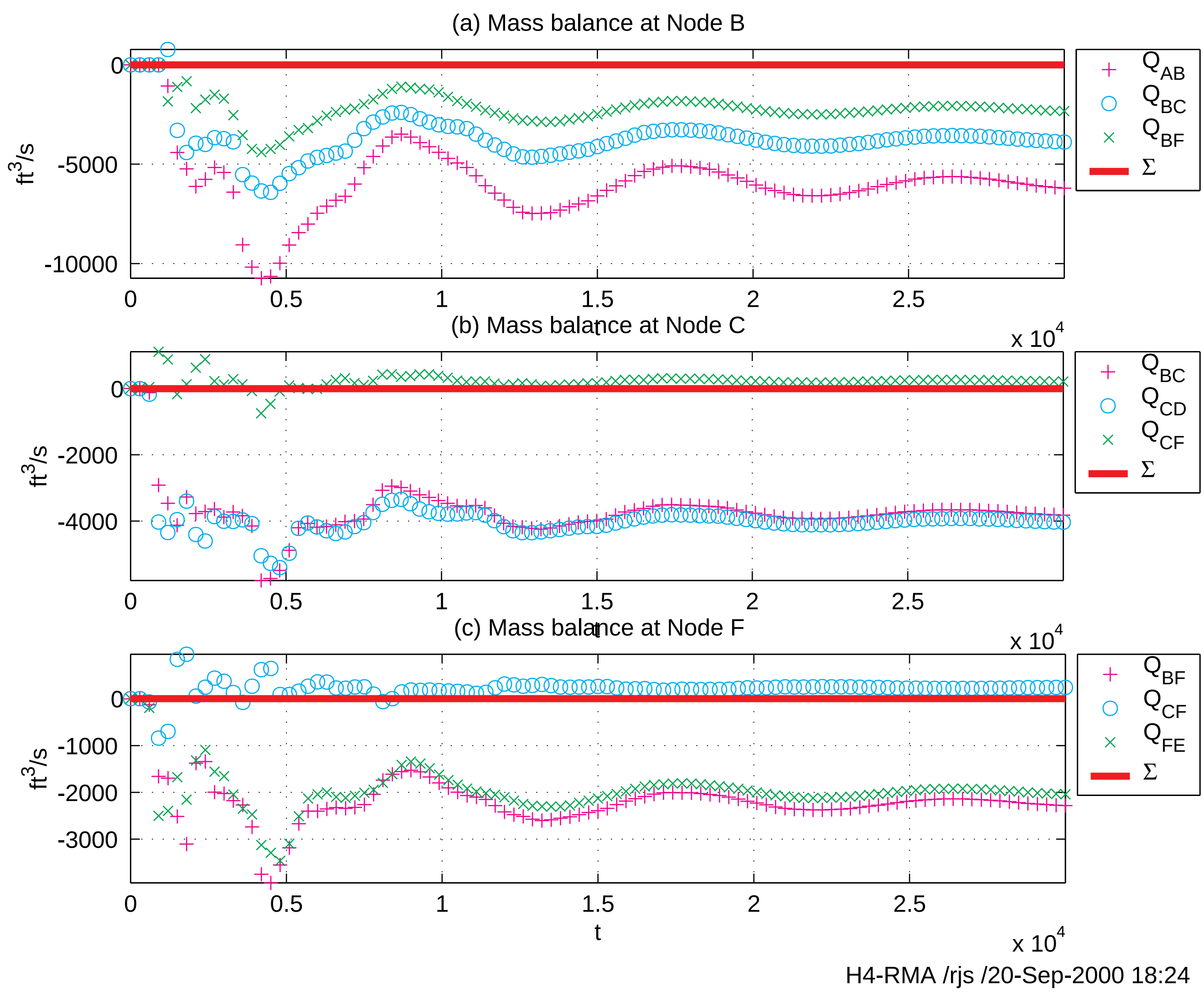

Figure 7.17: H4 RMA-predicted mass balances at network nodes.